A Large Targeted Deletion of *Hoxb1–Hoxb9* Produces a Series of Single-Segment Anterior Homeotic Transformations

Olga Medina-Martínez,* Allan Bradley,†'‡
and Ramiro Ramírez-Solis*'‡'§,[1]

*Institute of Biosciences and Technology, Texas A&M University System Health Sciences
Center, 2121 W. Holcombe Boulevard, Houston, Texas 77030; †Howard Hughes Medical
Institute, Department of Molecular and Human Genetics, and ‡Program in Developmental
Biology, Baylor College of Medicine, Houston, Texas 77030; and §Genes and Development
Program, The University of Texas–Houston Graduate School of Biomedical Sciences,
Houston, Texas 77030

Hox genes regulate axial regional specification during animal embryonic development and are grouped into four clusters. The mouse *HoxB* cluster contains 10 genes, *Hoxb1* to *Hoxb9* and *Hoxb13*, which are transcribed in the same direction. We have generated a mouse strain with a targeted 90-kb deletion within the *HoxB* cluster from *Hoxb1* to *Hoxb9*. Surprisingly, heterozygous mice show no detectable abnormalities. Homozygous mutant embryos survive to term and exhibit an ordered series of one-segment anterior homeotic transformations along the cervical and thoracic vertebral column and defects in sternum morphogenesis. Neurofilament staining indicates abnormalities in the IXth cranial nerve. Notably, simultaneous deletion of *Hoxb1* to *Hoxb9* resulted in the sum of phenotypes of single *HoxB* gene mutants. Although a higher penetrance is observed, no synergistic or new phenotypes were observed, except for the loss of ventral curvature at the cervicothoracic boundary of the vertebral column. Although *Hoxb13*, the most 5′ gene, is separated from the rest by 70 kb, it has been suggested to be expressed with temporal and spatial colinearity. Here, we show that the expression pattern of *Hoxb13* is not affected by the targeted deletion of the other 9 genes. Thus, *Hoxb13* expression seems to be independent of the deleted region, suggesting that its expression pattern could be achieved independent of the colinear pattern of the cluster or by a regulatory element located 5′ of *Hoxb9*. © 2000 Academic Press

Key Words: chromosomal engineering; *Hox* clusters; large targeted deletion.

INTRODUCTION

The 39 known mammalian *Antp*-like homeobox-containing (*Hox*) genes are clustered in four linkage groups (*HoxA, HoxB, HoxC,* and *HoxD*). Each group is located on a different chromosome in both mice and humans. These four mammalian *Hox* clusters are orthologues to the single cluster present in lower chordates like *Amphioxus* and in the non-Chordata phyla (García-Fernández and Holland, 1994). The four clusters appear to have evolved by multiple rounds of duplication and divergence from the original ancestral cluster in the tetrapod lineage (Kappen *et al.*,

1989; Bailey *et al.*, 1997). This evolutionary history is responsible for the fact that corresponding individual genes within the clusters share structural similarities across the clusters. Analysis of the nucleotide sequences of individual genes has produced 13 groups of genes that share a sufficient degree of similarity to be grouped in subfamilies, named the paralogous groups (reviewed in Krumlauf, 1994). Genes within these paralogous groups share not only structural similarities but also very similar, although not identical, expression patterns (Gaunt *et al.*, 1989).

Natural mutants in the mammalian *Hox* genes are scarce. In mice, hypodactyly (*Hd*) is caused by a deletion within the *Hoxa13* locus (Mortlock *et al.*, 1996); in humans, synpolydactyly is caused by an expansion of alanine-encoding triplets in the 5′ coding sequence of *HOXD13* (Muragaki *et*

---

[1] Current address: Lexicon Genetics, Inc., 4000 Research Forest Drive, The Woodlands, TX 77381.

al., 1996; Nurten Akarsu *et al.,* 1996). Otherwise, the function of *Hox* genes in mammals has been studied mainly through gain-of-function (Lufkin *et al.,* 1992; Argao *et al.,* 1995; Balling *et al.,* 1989; Charite *et al.,* 1995; McLain *et al.,* 1992; Wolgemuth *et al.,* 1989) and loss-of function experimental manipulations in transgenic mice. Loss-of-function experiments have consisted mostly of individual gene mutations generated by gene targeting in embryonic stem (ES) cells (Barrow and Capecchi, 1996; Carpenter *et al.,* 1993; Chen and Capecchi, 1997; Chen *et al.,* 1998; Chisaka and Capecchi, 1991; Chisaka *et al.,* 1992; Condie and Capecchi, 1993; Goddard *et al.,* 1996; Godwin and Capecchi, 1998; Horan *et al.,* 1994; Kostic and Capecchi, 1994; Le Mouellic *et al.,* 1992; Lufkin *et al.,* 1991a; Mark *et al.,* 1993; Ramirez-Solis *et al.,* 1993; Rijli *et al.,* 1993; Saegusa *et al.,* 1996; Studer *et al.,* 1996; Suemori *et al.,* 1995). This extensive mutational analysis has demonstrated that *Hox* genes are implicated in the regulation of segmental identity along the axial vertebral column, the hindbrain, and the limb proximodistal axis. The development of several organs is also regulated by Hox gene products. For example, members of the ninth paralogous group are important for mammary gland development during pregnancy (Chen and Capecchi, 1999), *hoxb4* and/or *hoxb2* are important for sternum development (Barrow and Capecchi, 1996; Ramirez Solis *et al.,* 1993), and members of the third paralogous group play a role in thymus, thyroid, and parathyroid gland development (Manley and Capecchi, 1995, 1998).

The study of mice carrying mutations in multiple *Hox* genes has revealed a complex network of interactions among genes from different clusters to regionalize the embryo. Double and triple mutants have been generated through the intercrossing of individual targeted mutations (Manley and Capecchi, 1997; Chen and Capecchi, 1997; Chen *et al.,* 1998; Condie and Capecchi, 1994; Davenne *et al.,* 1999; Fromental-Ramain *et al.,* 1996; Horan *et al.,* 1995b; Manley and Capecchi, 1998). This approach is particularly important since the similarities within paralogous groups increase the likelihood that paralogous genes could compensate for the loss of an individual gene. Indeed, the combination of two or three mutations in the same animal demonstrates that individual Hox proteins from the same paralogous groups have redundant and nonredundant functions, as well as synergistic interactions (Chen and Capecchi, 1997; Chen *et al.,* 1998; Horan *et al.,* 1995a,b). To generate mice carrying multiple mutations in the same linkage group could be done by multiple rounds of gene targeting or by the simultaneous deletion of several genes. This is necessary because the short distance between the genes in the clusters precludes the combination of individual mutations by intercrossing individual mutants. Few examples of such double and triple mutations have been reported; simultaneous deletion of *Hoxd11, Hoxd12,* and *Hoxd13* causes synpolydactyly in mice (Zakany and Duboule, 1996). The intercrossing of individual mutants for genes from the same cluster leads to the production of *trans*-heterozygotes, which reduces (but does not eliminate)

the dosage of two genes. For example, analysis of *trans*-heterozygotes has led to the suggestion that *hoxb5* and *hoxb6* possess a nonallelic–noncomplementation genetic interaction to regionalize the cervicothoracic boundary of the vertebral column (Rancourt *et al.,* 1995).

The *HoxB* cluster on mouse chromosome 11 contains 10 known genes distributed over approximately 170-kb. The first 9, *Hoxb1* to *Hoxb9,* occupy about 100 kb (Rubock *et al.,* 1990), while the last, *Hoxb13,* is located approximately 70 kb upstream of the *Hoxb9* gene (Zeltser *et al.,* 1996). As in all the mammalian *Hox* clusters, the *HoxB* genes have the same transcriptional orientation, the 5' end toward *Hoxb13* and the 3' end toward *Hoxb1.* In addition, all of them, even *Hoxb13,* maintain the same properties of spatial and temporal colinearity as the rest of the *Hox* genes. Genes located toward the 3' end (i.e., *Hoxb1*) are expressed earlier during development (temporal colinearity) and more anterior along the anteroposterior embryonic axis (spatial colinearity) than genes located toward the 5' end (i.e., *Hoxb13*) (Duboule and Dolle, 1989; Duboule and Morata, 1994; Gaunt *et al.,* 1988; Graham *et al.,* 1989). Despite important recent advances (Kondo and Duboule, 1999; Kondo *et al.,* 1998; van der Hoeven *et al.,* 1996; Zakany *et al.,* 1997) the molecular mechanism(s) of colinearity remains virtually unknown.

Here, we report the phenotype of mutant mice carrying a large targeted deletion in the *HoxB* cluster. The deficiency, *del(11) (HoxB1-HoxB9)[Brd]* (from now on referred to as *HoxBΔ1*), eliminates simultaneously all the genes between and including *Hoxb1* and *Hoxb9. HoxBΔ1* was generated through chromosomal engineering, a technique that permits the introduction of large targeted deficiencies into the mouse germ line (Liu *et al.,* 1998; Ramirez-Solis *et al.,* 1995). Unexpectedly, the heterozygous mice show no phenotype and are fertile. Homozygous embryos survive until late in gestation and die after delivery, most likely by their inability to breathe. Skeletal analysis reveals no phenotype in the heterozygotes and a series of single-segment anterior homeotic transformations along the vertebral column between the first cervical and the eighth thoracic vertebra in the homozygous mutants. The sternal bands are small and separate, and whole-mount neurofilament staining reveals defects in the cranial nerves. Whole-mount RNA *in situ* hybridization analysis of *Hoxb13* expression shows no difference between the deficient mice and their wild-type littermates, demonstrating that the colinearity mechanism employed by *Hoxb13* does not require any element included within the deletion.

MATERIALS AND METHODS

Chromosomal Engineering to Generate Targeted Deletion at the HoxB Cluster

A replacement-type targeting vector for the 3' end of the *HoxB* cluster consisted of a 3.5-kb *BglII–NcoI* 5' homologous arm and a 2.1-kb *BglII–PvuII* 3' homologous arm. The vector arms were
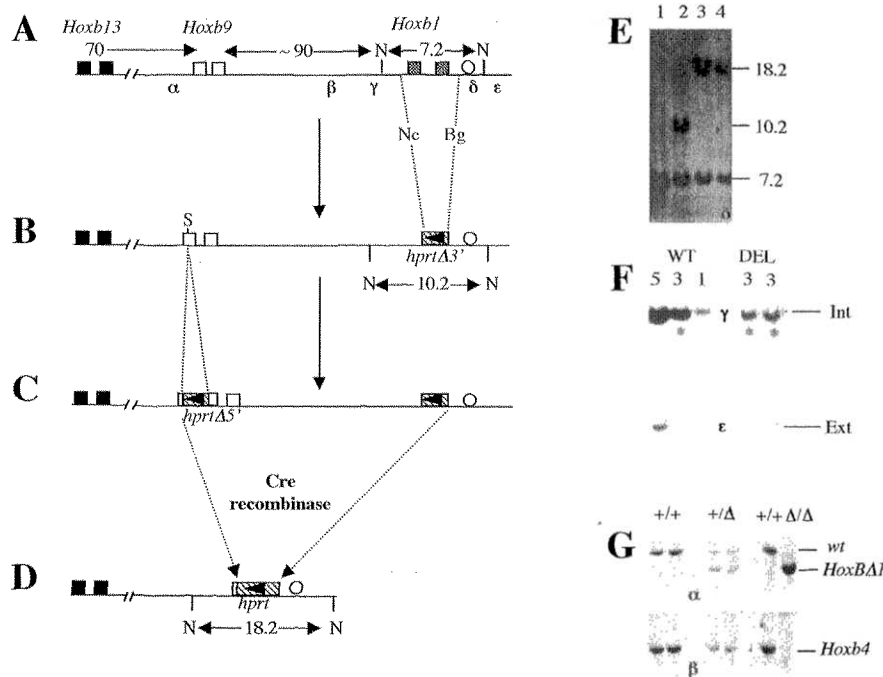
FIG. 1. Chromosomal engineering (CE) strategy to delete the genes from *Hoxb1* to *Hoxb9*. (A) Schematic representation of the *HoxB* cluster. Numbers between arrows indicate the distance between the *Hox* genes in kilobases; boxes (black, white, or stippled) represent the exons of the *Hoxb13, Hoxb9,* and *Hoxb1* genes; and the white circle represents the 3' retinoic acid-responsive element which participates in the regulation of *Hoxb1*. Greek letters below the cluster represent DNA fragments used as probes (described in detail under Materials and Methods.) N represents *Nhe*I restriction enzyme sites surrounding the *Hoxb1* gene. (B) In the first step of CE, the *hprt*Δ3' replaced *Hoxb1* between the *Nco*I (Nc) and *Bgl*II (Bg) restriction sites. The *hprt*Δ3' cassette contains a partial and nonfunctional *hprt* minigene (striped box) that includes a *loxP* site (black arrowhead). (C) In the second step of CE, an ES cell clone with the *Hoxb1*-targeted gene was identified by Southern blot analysis and used to target the *Hoxb9* locus with the *hprt*Δ5' cassette at the *Sal*I site in exon 1. The *hprt*Δ5' cassette contains a partial and nonfunctional *hprt* minigene (striped box) complementary to *hprt*Δ3' which also includes a *loxP* site (black arrowhead.) The arrowheads also indicate the relative direct orientation of the *loxP* sites. (D) Double-targeted ES cells were expanded and transiently transfected with a Cre expression cassette. Cre-mediated recombination reconstitutes a functional *HPRT* minigene while it deletes the intervening sequences (90 kb). (E) Southern blot analysis of the *Hoxb1–Hoxb9* CE deletion. Genomic DNA from wild type, double targeted, and two representative *HoxB*Δ*1* clones was restriction digested with *Nhe*I and hybridized to the external probe δ. The wild-type band is 7.2 kb, which changes to 10.2 kb upon gene targeting at the *Hoxb1* locus and then to 18.2 kb upon Cre-mediated recombination. (F) Gene dosage of internal (deleted) and external (nondeleted) probes. 5, 3, and 1 μg of genomic DNA from wild-type ES cells (WT5, WT3, and WT1, respectively) and 3 μg of genomic DNA from two representative *HoxB*Δ*1* ES cell clones (DEL) were analyzed by Southern blot with probes γ (Int) and ε (Ext). All the DNAs were quantitated after restriction digest. Probe ε demonstrates that the amount loaded for each of the *HoxB*Δ*1* clones is 3 μg, but probe γ produces a reduced signal intensity, presumably half the dosage (equivalent to 1.5 μg of the wild type). (G) Southern blot analysis of the *HoxB*Δ*1* allele after germ-line transmission. Tail genomic DNA corresponding to the genotypes indicated (top) was cut with the restriction enzyme *Eco*RI and analyzed with the diagnostic probe α (upper blot). The upper band (12 kb) and the lower band (6 kb) represent the wild-type and mutant alleles, respectively. The blot was stripped and rehybridized with probe β (*Hoxb4*) (lower blot). The last lane corresponds to a homozygous *HoxB*Δ*1* individual and shows the absence of signal from the *Hoxb4* locus (deleted).

separated by the *hprt*Δ3' cassette (Ramirez-Solis *et al.,* 1995) that replaces a 1.7-kb *Nco*I–*Bgl*II region which includes both exons and the intron of the *Hoxb1* gene. This targeting vector was electroporated into AB2.2 ES cells under standard conditions (Ramirez-Solis *et al.,* 1993). G418 selection was applied 24 h after electroporation and G418-resistant ES clones were screened for the targeted integration event by Southern blot analysis as described (Ramirez-Solis *et al.,* 1992) (data not shown).

One ES cell clone that contained the correct integration of the *hprt*Δ3' cassette at the *Hoxb1* locus (Figs. 1A and 1B) was used as substrate to electroporate a targeting vector directed to *Hoxb9*. An insertion-type targeting vector was built using a 6.6-kb *Hind*III fragment that includes the two exons of the *Hoxb9* gene interrupted by an insertion of the *hprt*Δ5' cassette (Ramirez-Solis *et al.,* 1995) into the unique *Sal*I site present in the first exon. This vector was electroporated and ES cells were selected for resistance to puromycin. Ten days after the electroporation, ES cell clones were screened for gene targeting at the *Hoxb9* locus by Southern blot analysis.

Double-targeted ES cells were electroporated with Cre expres-

sion plasmid (pOG231). Two days after electroporation, HAT selection was applied and resistant colonies were isolated, expanded, and analyzed by Southern blot (Ramirez-Solis et al., 1992). HAT resistance was gained by the recombination of the directly repeated loxP sites included in the hprtΔ3' and hprtΔ5' cassettes. Changes produced by each one of the recombination events were confirmed by Southern blot analysis using different probes. Probes used in this analysis and their relative positions are indicated in Fig. 1A. Alpha (α) is an external probe located 5' of Hoxb9 gene that is diagnostic for the targeted integration of the hoxb9-hprtΔ5' vector (EcoRI digest) and for the HoxBΔ1 deletion (NheI or EcoRI digests.) Beta (β) is a probe derived from the Hoxb4 locus that shows that the internal sequences have been deleted. Gamma (γ) is a probe located inside the deletion which is located just upstream of Hoxb1. Delta (δ) is an external probe located 3' of Hoxb1 but inside the NheI fragment that contains it; it is diagnostic for the targeted integration of the hoxb1-hprtΔ3' cassette and for the new junction fragment after the Cre-mediated HoxBΔ1 deletion. Epsilon (ε) is an external probe used a control in the gene dosage experiments (Fig. 1E.)

Germ-Line Transmission and Genotypic Analysis

Heterozygous HoxBΔ1 ES cells were injected into C57BL/6J blastocysts to generate chimeric males. Chimeric males were bred to C57BL/6J females to introduce the mutation into the germ line. F_1 heterozygous mice were intercrossed to generate homozygous mutants.

Genomic DNA was prepared from the tails of adult or newborn mice or from the yolk sac of embryos by overnight digestion with proteinase K followed by ethanol precipitation. The DNA was digested with EcoRI and analyzed by Southern blot and hybridization with the ^{32}P-labeled probe α (located 5' of Hoxb9 as described above.)

Skeletal Analysis of HoxBΔ1 Mutants

Newborn mice were euthanized by CO_2 inhalation and whole-mount skeletal preparations were made by the alizarin red/Alcian blue method as described (Lufkin et al., 1991b). To finish the preparations, the skeletons were dehydrated in methanol and cleared in a mix of benzyl alcohol:benzyl benzoate 1:1 prior to photography on a Nikon SMZ-U microscope.

Histology

Mouse embryos were fixed in Bouin's solution overnight at room temperature and embedded in paraffin by standard methods. Serial sections (7 μm) were prepared and stained with hematoxylin–eosin.

Hoxb13 Whole-Mount RNA in Situ Hybridization

Mouse embryos of 8.5 and 9.5 days postcoitus (E8.5 and E9.5, respectively) were dissected and fixed with 4% paraformaldehyde. The yolk sac was used to prepare genomic DNA for genotype analysis. Whole-mount RNA in situ hybridization was performed using a standard protocol (Wilkinson and Nieto, 1993). The probe used for the in situ analysis was a 650-bp DNA fragment containing part of the first exon of Hoxb13. This probe was labeled with digoxigenin by in vitro transcription.

Hoxb13 RT-PCR

Mouse embryos (E8.5 and E9.5) were dissected in PBS. Total RNA was extracted from pooled embryos or embryo parts (trunks or heads from E9.5 embryos) with a commercial reagent (Ultraspec). Reverse transcription (RT) was performed with SuperScript reverse transcriptase and random hexamer primers. Ten percent of each reverse-transcribed sample was used as template for the polymerase chain reaction (PCR). Two different sets of PCR primers were used. The first set was 5'-ATGGAGCCCGGCAATT-3' and 5'-TCACGGGGTAGTGCTGG-3' (reverse). The second set was 5'-TTACCTGGATGTGTCTGTGG-3' and 5'-TTGCGCCTC-TTCTCCTTAGT-3' (reverse). One-quarter of the reaction was separated by electrophoresis on 1% agarose gel and analyzed by Southern blot using a ^{32}P-labeled Hoxb13 internal probe. Control for the integrity of the RNA and the efficiency of reverse transcription was provided by amplification of β-actin and BMP-4 positive controls (data not shown).

Immunohistochemistry

Whole-mount preparations of the nervous system of E10.5 embryos was performed by immunohistochemistry with antibody 2H3 (anti-155-kDa neurofilament protein) (Developmental Studies Hybridoma Bank) using a standard protocol (Wall et al., 1992).

RESULTS

Generation of HoxBΔl Mutant Mice

ES cells carrying a targeted deletion including the nine genes from Hoxb1 to Hoxb9 of the HoxB complex were generated using chromosomal engineering as summarized in Fig. 1. The HoxBΔ1 deletion was introduced into the mouse germ line by breeding chimeric males to C57BL/6J females. Therefore, all the data contained in this report were obtained in a mixed genetic background C57BL/6J and 129SvEvBrd. F_1 heterozygous mice were normal, healthy, and fertile, and no deviation from Mendelian expectations was noticed in the progeny derived from the ES cell component of the chimera.

HoxBΔ1 Mutants Complete Embryogenesis but Die at Birth

Mice heterozygous for the HoxBΔ1 mutation were bred to produce homozygous F_2 progeny. The F_2 progeny was obtained with a 1:2:0 (+/+:+/−:−/−) distribution when the genotype was obtained at 3 weeks of age, indicating again that the heterozygotes survive but that the homozygous HoxBΔ1 mutants die before weaning (Table 1). No homozygous mutants were recovered after 2 days of age but some dead mutants were recovered on the first day after delivery. Embryo dissection and genotype analysis at different embryonic stages (E9.5–E18.5) indicate that most, if not all, homozygous mutants complete embryogenesis and die very late in development, possibly right after delivery.

All mutant newborn mice had a characteristic rounded body shape with the head tilted into the thorax (Fig. 2A).

TABLE 1

Genotype Ratio for *HoxBΔ1* Mice

Age	n	+/+	+/Δ	Δ/Δ
E9.5	9	2	4	3
E10.5	40	9	20	11
E11.5	14	2	9	3
E12.5	11	1	6	4
E13.5	28	7	18	3
E14.5	17	7	6	4
E15.5	16	5	6	5
E16.5	24	9	9	6
E17.5	17	5	9	3
E18.5	44	10	19	15
Newborn	24	6	7	11[a]
2 day old	29	12	17	0
Weaning	18	5	13	0

[a] All were found dead in the cage.

Although the skin is closed in the ventral side of the thorax, the abdominal wall and the sternal bands are open in all the *HoxBΔ1* mutants (Fig. 2B). Autopsy revealed no obvious morphological abnormalities of the major organs, including lungs, liver, kidneys, and spleen. However, mutant mice sometimes showed internal hemorrhages in the dorsolateral region of the neck and edema, suggesting a cardiovascular malfunction. Examination of whole-mount skeletal preparations revealed very small (50% normal size) and nonfused sternal bands. The open sternal bands show a reduced number and size of sternebrae (Fig. 2C).

Histological Analysis of HoxBΔ1 Mice

Histological sections were made on E16.5 embryos to gain further insight into the defects in the thoracic cavity (Fig. 2D). Sagittal section of the mutant embryo reveals the absence of the ventral curvature of the vertebral column that is normally present at the cervicothoracic boundary. On the ventral side, the sternum is not observed although the skin is closed. The thoracic cage of the mutant is also much smaller. The size of the thorax and the rounded shape of the mutant embryo could be due to the much shorter distance between the fold of the neck and the diaphragm's ventral attachment compared to their control wild-type littermates (Fig. 2D). In turn, this could be due to the small size of the sternal bands.

Mutant embryos showed atrial and ventricular heart chambers similar to those of their wild-type littermates, but exhibited an increase in size and a change in relative position of the heart in the thorax. Sagittal sections of E16.5 embryos revealed that the heart and some of the great vessels are enlarged and malformed (Fig. 2D) compared to wild-type and heterozygous littermates. This abnormality could be related to the edema and hemorrhages detected in some embryos and be a secondary consequence of the

hypoplastic and open sternum since the embryos that show these signs were never recovered before E14.5, the first time that obvious sternum abnormalities are displayed. Consistent with this, histological sections of mutant hearts at E9.5 revealed no evident abnormalities (data not shown).

Additionally, other organs (i.e., thyroid gland, thymus, etc.) appear normal in size but show an abnormal shape. Again, we assume that this is a secondary effect of the changes of the thoracic rib cage in the *HoxBΔ1* mutants. Consistent with this, the single mutation of *Hoxb9* leads to a reduction in the size and an alteration in the shape of the thymus. This phenotype appears to be associated with fusions of the most anterior ribs since in *hoxb9* mutants lacking the fusions the thymus is normal (Chen and Capecchi, 1997). Detailed analysis of the role of *Hox* group 3 paralogous genes has demonstrated that *Hoxb3* mutants do not show defects in the thymus even though double mutants for *Hoxa3–Hoxb3* showed exacerbation of defects previously associated with *Hoxa3* individual mutation (Manley and Capecchi, 1995, 1998).

Homeotic Phenotypes

Skeletal analysis in heterozygous embryos (n = 44) revealed no differences from their wild-type littermates. Absence of phenotype in the heterozygous mice is surprising because studies of *hoxb5⁻* and *hoxb6⁻* transheterozygous mice (Rancourt *et al.*, 1995) have suggested that both genes are required for a common function, implying that the dosage or relative levels of these two genes are critical. However, we could not document any gene dosage-dependent skeletal phenotype in the *HoxBΔ1* heterozygotes, demonstrating that genetic interactions between members of the cluster previously inferred do not occur.

Mutant skeletons reveal various abnormalities along the cervical and thoracic regions of the vertebral column (n = 30 +/+, 44 +/Δ, and 20 Δ/Δ) (Δ, *HoxBΔ1*) (Fig. 3). Abnormalities observed in the cervical region include a thinner neural arch on the first cervical vertebra (C1) and thickening of the neural arch of C2, sometimes carrying a reminiscent extra ventral tubercle (12%) (Fig. 3A). No abnormalities were detected in the third to fifth cervical vertebrae (C3–C5) in the *HoxBΔ1* homozygous mutants. The sixth cervical vertebra (C6) normally has two bilateral ventral projections known as anterior tuberculi (Fig. 3B). In all the mutants, one or both anterior tuberculi were absent or fused with an abnormal ectopic tuberculi present on C7. The C7 vertebra of all the mutants exhibited one or two ectopic anterior tuberculi sometimes fused to tuberculi present on C6 (Figs. 3A and 3B). The mutant C7 also showed vertebrarterial canals, which are normally only on vertebrae C1 to C6 (Fig. 3B). In wild-type mice, the first rib (R1) arises from the first thoracic vertebra (T1) and grows ventromedially to contact the top of the sternum. In *HoxBΔ1* mice, R1 was reduced or even absent on one or both sides and was no longer connected to the sternum so that T1 resembled C7 (Fig. 3B). If present, R1 formed a small
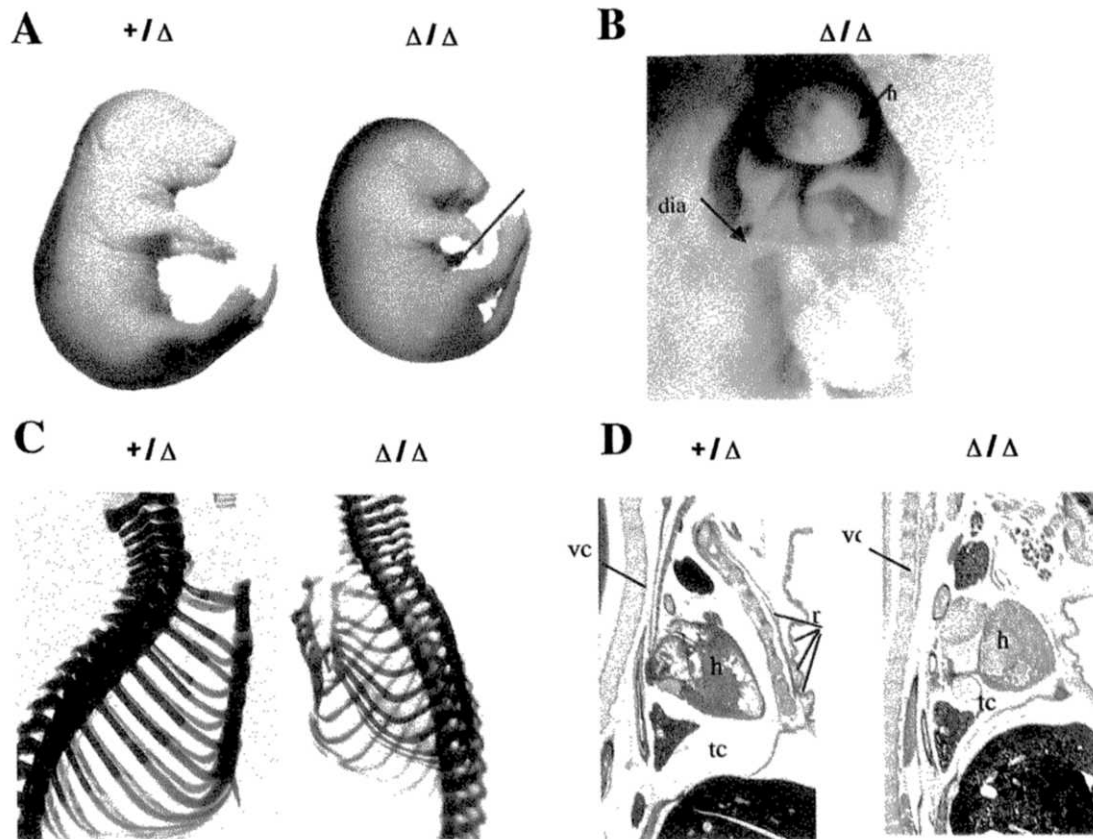
FIG. 2. General features of the *HoxBΔ1* mutant mice. Genotypes are indicated at the top; Δ, *HoxBΔ1*. (A) External appearance of newborn mice. The *HoxBΔ1* homozygous newborns have a characteristic rounded body shape with the head tilted toward the thorax and defects in the closure of the abdominal wall, which often exhibits protruding intestines (pi). (B) Frontal view of mutant newborn mice. Dissection of the skin shows the open sternum with the heart (h), lungs, and diaphragm (dia). (C) Thoracic skeletal analysis of the *HoxBΔ1* mutants. The mutant sternum is split, and the unfused sternal bands are half the normal size. The number of sternebrae is reduced possibly as a consequence of the closeness of the sternocostal junctions. (D) Near-sagittal histological sections of the thoracic cage (tc). Dorsal is to the left. The absence of the ventral curvature of the vertebral column is evident in the mutant (vc). Transverse sections through the ribs can be observed in the ventral side of the heterozygous control. In the mutant, the ventral skin is closed but there is no skeleton (ribs nor sternum) between the skin and the heart. The distance between the neck fold and the ventral attachment of the diaphragm is much shorter in the mutant than in the control. The heart (h) and great vessels show defects of position and size.

rib that often fused to the second rib (R2). The second rib (R2) in the mutants joined the top of the sternal bands, similar to the wild-type R1 (Fig. 3C). In wild-type mice, the R2 sternocostal joint is well separated from that of R1 and is the most anterior to show inhibition of ossification during sternum morphogenesis (Chen, 1952). In the mutants, the first sternebra lay between the third rib (R3) and R2, similar to the normal position between R2 and R1 in wild-type mice (Fig. 3C). Normally, only the first seven ribs (R1–R7) form joints with the sternum, but in the mutants, the eighth rib (R8) appeared unusually long and sometime joined the sternal bands on one or both sides, resembling the normal R7 (Fig. 3C). No additional phenotypes were observed in more posterior regions. All these changes can be interpreted as a series of anterior homeotic transformations involving two neighboring vertebrae along the cervical and thoracic region of the axial skeleton.

Interestingly, no posterior transformations were detected in the *HoxBΔ1* mutant mice, which is consistent with Lewis' model for *Hox* gene action in flies (Lewis, 1978) and contrasts with posterior transformation phenotypes caused by individual mutations of some *Hox* genes (Horan *et al.*, 1994; Jeannotte *et al.*, 1993; Kostic and Capecchi, 1994). Thus, our data indicate that the Lewis model seems to be applicable for *Hox* gene function even in vertebrates. Additionally, our results strongly support the idea that some posterior phenotypes of single-gene mutants might be artifactual gain of function by the resistance markers used during gene targeting (Fiering *et al.*, 1993, 1995).

As shown in Fig. 3D, although *HoxBΔ1* increases the
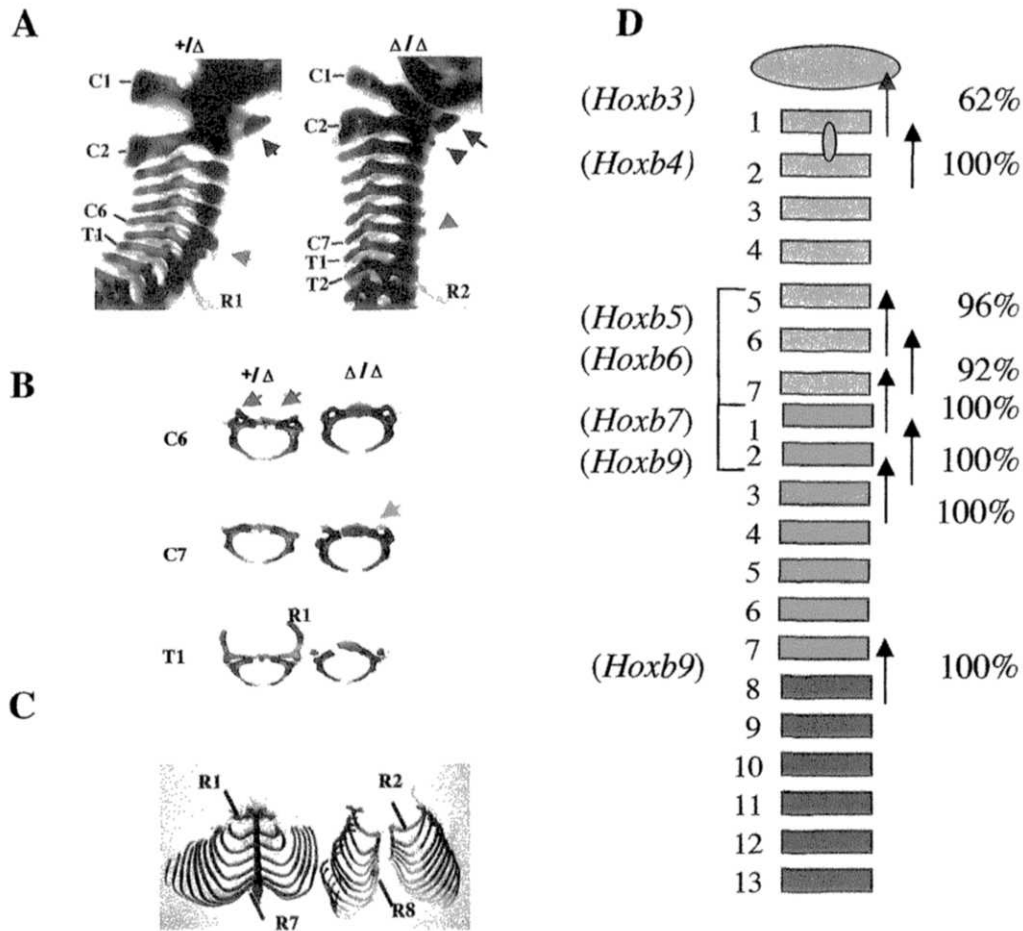
FIG. 3. Series of anterior homeotic transformations along the vertebral column in *HoxBΔ1* mice. Genotypes are indicated at the top. (A) Lateral view of cervical skeleton. Dorsal is to the left. Cervical (C1, C2, C6, C7) and thoracic (T1, T2) vertebrae are as numbered. C1/C2 ventral tubercle (black arrowhead) and C6/C7 ventral tubercles (blue arrowhead) are indicated. Heterozygous mice display a wild-type morphology and are used as controls. *HoxBΔ1* homozygous mice show diverse abnormalities, including a thinner neural arch on C1 and thickening of the neural arch of C2, which often carries a reminiscent ventral tubercle. Additionally, anterior tuberculi normally present on C6 were absent and present ectopically on C7. The absence of the normal ventral neck curvature is again evident. (B) Coronal view of the dissected C6, C7, and T1 vertebrae. *HoxBΔ1* mutants show C6 lacking anterior tubercles and C7 presenting ectopic vertebrarterial canals (red arrowhead.) The left canal is incomplete but the right one is complete. The first rib pair (R1) in the mutant T1 vertebra is reduced to a pair of stumps. (C) Ventral view of dissected rib cage. The mutant rib cage shows absence of R1 and formation of an ectopic sternocostal joint between the second rib pair (R2) an the top of the sternal bands. The sternocostal joints of the R2 and R3 are separated by the first sternebra, characteristically larger than the others. This feature is normally present between the sternocostal joints of R1 and R2. The mutant 8th rib (R8) is long and often forms an ectopic sternocostal junction. Again, the mutant sternal bands can be seen, short and separated. (D) Schematic representation of the transformations observed in the *HoxBΔ1* mutant. Numbered rectangles represent cervical (blue), thoracic with ribs that attach to the sternum (red), and thoracic with free-floating ribs (green) vertebrae. The anterior homeotic transformations observed in the *HoxBΔ1* mutants are indicated by upward arrows and their penetrance in a 129SvEv/C57BL/6J hybrid genetic background is indicated on the right. On the left, there is a list of the potential genes involved in each of the transformations according to the published literature.

penetrance of homeotic transformation, the abnormalities observed at the axial skeleton are equivalent to the sum of individual *HoxB* gene loss-of-function mutants. These observations suggest that although there is functional compensation between genes of the *HoxB* cluster, at least at the axial level no novel additional phenotypes are present when mutants alleles on the same cluster are combined.

Effects of HoxBΔ1 in Cranial Nerve Patterning

Analysis of *Hoxb1*, *Hoxb2*, and *Hoxb3* individual null mutants has shown that these genes are involved in hindbrain specification (Goddard *et al.*, 1996; Studer *et al.*, 1996; Barrow and Capecchi, 1996; Manley and Capecchi, 1997). To investigate if cranial nerves and associated ganglia are

TABLE 2
Summary of Cranial Nerve Defects in *HoxBΔ1* Mutants

	+/+ (n = 3)	+/Δ (n = 12)	Δ/Δ (n = 11)
Nerve			
IV Trochlear	Normal	Normal	Normal
V Trigeminal	Normal	Normal	Normal
VI Abducens	Normal	Normal	Normal
VII Facial	Normal	Normal	Normal
VIII Acoustic	Normal	Normal	Normal
IX Glossopharyngeal	Normal	Normal	Closer to X unilateral (3)
			Closer to X bilateral (1)
			Absent unilateral (2)
X Vagus	Normal	Normal	Abnormal migration (1)[a]
Ganglia			
Vg Trigeminal	Normal	Normal	Normal
VII/VIII Facioacustic	Normal	Normal	Normal

[a] This mutant also lacks the IX nerve.

affected in *HoxBΔ1* mice, we analyzed E10.5 embryos by whole-mount immunostaining of neurofilaments. Heterozygous mice, immunostained with 2H3 antineurofilament antibody, were indistinguishable from wild-type littermates. Detailed analysis of cranial nerves in *HoxBΔ1* homozygotes showed defects involving the glossopharyngeal (IXth) and the vagal (Xth) nerves with low penetrance and variable expressivity, even between the two sides of the same embryo. No further patterning defects in other cranial nerves (summarized in Table 2) were detected with this method. Two embryos, of 11 examined, lacked the IXth nerve unilaterally (Fig. 4B) and others (4/11) showed the IXth nerve abnormally fused to the Xth nerve (vagal) (Fig. 4C). These abnormalities are similar to those previously described for the null mutation of *Hoxb3* (Manley and Capecchi, 1997). These results suggest that despite the combined lack of four different *HoxB* genes that are expressed in the hindbrain (*Hoxb1, Hoxb2, Hoxb3, and Hoxb4*) no phenotypes are present other than those previously described for individual mutations. This result is clearly in contrast to the extensive synergy observed between paralogous genes, i.e., *Hoxa1/Hoxb1* in patterning the cranial nerves (Gavalas *et al.*, 1998). A detailed histological analysis of motor nuclei organization (i.e., VIIth motor nucleus is absent in *hoxb2* mutants) and a study of axonal projection by retrograde labeling and use of rhombomere markers will be necessary to address possible genetic interactions between *HoxB* genes in hindbrain specification.

Hoxb13 Gene Expression in HoxBΔ1 Mutant Mice

The *HoxBΔ1* deletion allele was generated before the *Hoxb13* gene was discovered (Zeltser *et al.*, 1996), and it does not include it (Fig. 1A). In contrast to the *HoxA, HoxC,* and *HoxD* clusters, which contain around four or five

duplicated *AbdB*-related genes, the *HoxB* cluster has only two known *AbdB* homologs (*Hoxb9* and *Hoxb13*). *Hoxb13* gene is located unusually far from the complex, 70 kb upstream of *Hoxb9*, but its expression pattern seems to maintain spatial colinearity despite the large distance that separates it from the rest of the *HoxB* cluster (Zeltser *et al.*, 1996). Since *Hoxb13* maintains its colinearity, we investigated whether the *HoxBΔ1* deficiency would produce alterations in its expression pattern, that is, if there is any sequence inside the deficiency that is required to establish/maintain spatial colinearity or if the colinear properties could be modified by bringing the *Hoxb13* locus and its surroundings 90 kb closer to the 3' end of the *HoxB* cluster. Whole-mount RNA *in situ* hybridization of *Hoxb13* at E9.5 revealed no significant difference between the mutants and their heterozygous or wild-type littermates (n = 5 +/+, 4 +/Δ, 8 Δ/Δ). The expression of *Hoxb13* is confined to the posterior aspects, i.e., the tail bud (Fig. 5A), suggesting that the relocation of the *Hoxb13* gene with respect to the 3' side of the cluster is not important for its correct spatial expression and that its expression pattern does not depend on any sequence inside the *HoxBΔ1* deficiency.

Next, we attempted to detect a change in the temporal expression of *Hoxb13* in the *HoxBΔ1* mutants. First, to define the earliest time at which *Hoxb13* expression was detected, we performed whole-mount RNA *in situ* hybridization at E8.5. No expression was detected at this stage in either mutant or wild-type embryos (data not shown). To increase the sensitivity of our assay, we performed RT-PCR to detect *Hoxb13* mRNA. RT-PCR with two different sets of primers detected *Hoxb13* expression at E8.5 in the trunk of the embryo (but not the head) for all genotypes, narrowing the time window to determine if the temporality has been affected (Fig. 5B). Thus, we were not able to document any difference of *Hoxb13* expression caused by the *HoxBΔ1* allele.

DISCUSSION

Nonallelic Noncomplementation at the HoxB Cluster?

Here, we analyzed the effects of a targeted deletion in the murine *HoxB* complex that eliminates all the *HoxB* genes between and including *Hoxb1* and *Hoxb9*, but not *Hoxb13*. Heterozygous *HoxB∆1* mice are normal and therefore allowed us to generate and analyze *HoxB∆1* homozygous mutants. Previous studies have suggested the existence of important gene dosage relationships between members of the *HoxB* cluster. Analysis of *trans*-heterozygotes between individual mutants for *hoxb5* and *hoxb6* suggests that these two loci may have a genetic relationship of nonallelic noncomplementation (Rancourt *et al.*, 1995). Briefly, both genes are important for specification of the identity of the vertebral column between C6 and T1, and such function is sensitive to the combined gene dosage ($2X + 2X$ in the wild-type animal.) In heterozygotes for the individual mutations, the dosage ($2X + 1X$) would be sufficient for the correct development of the vertebrae, but in *trans*-heterozygotes ($1X + 1X$), or in mice homozygous for any individual mutation of both genes ($2X$), the gene product would not be sufficient for proper function. If this were the case, the heterozygous *HoxB∆1* mutants, in which the level of *hoxb5* and *hoxb6* product would be reduced the same as in the *trans*-heterozygotes ($1X + 1X$), should exhibit the phenotype. Unexpectedly, the *HoxB∆1* heterozygous mice show no detectable phenotype, and thus our results are inconsistent with the nonallelic noncomplementation model proposed for *Hoxb5* and *Hoxb6* genetic interactions. One explanation for the nonallelic noncomplementation could be that the function of other genes removed by our deletion is required for that phenotype. Another explanation for the phenotype of the *hoxb5–hoxb6 trans*-heterozygotes could be that both targeted mutations affect a common gene (*hoxb5*, *hoxb6*, or another) and that this *common mutation* is brought to homozygosity in the *trans*-heterozygous mice. This possibility is raised by the documented effect of drug resistance cassettes around a targeted locus (Fiering *et al.*, 1993, 1995) and by the complex transcriptional regulation in the *Hox* clusters (i.e., multiple promoters, overlapping transcription units, overlapping tissue-specific enhancers) (Gould *et al.*, 1997; Sham *et al.*, 1992; Sharpe *et al.*, 1998; Whiting *et al.*, 1991). Indeed, effects of targeted mutations on neighboring genes have been documented previously (Barrow and Capecchi, 1996; Rijli *et al.*, 1994). Detection of artifactual effects on the expression of neighboring genes could be extremely difficult since it would require knowledge of the precise time, level, and place of expression that is important for the function of the gene involved.

Hox Code and Homeotic Phenotypes

HoxB∆1 homozygous mutants show a series of abnormalities in the vertebral pattern that can be interpreted as single-segment anterior-only homeotic changes. These homeotic transformations represent a series of anterior transformations as were defined by Lewis (1978). Lewis' model for *Hox* action in *Drosophila* predicts that ectopic expression of *Hox* genes might lead to a posterior homeosis, whereas loss of *Hox* gene function leads to anterior transformation (Lewis, 1978). This correspondence has been extended to vertebrates by studies in which homeotic transformations were correlated to modulation of *Hox* gene expression (Kessel *et al.*, 1990; Kessel and Gruss, 1991; Wright *et al.*, 1989). However, experiments intended to generate null alleles of some individual *Hox* genes exhibit posterior transformations (Jeannotte *et al.*, 1993; Small and Potter, 1993; Horan *et al.*, 1994). Interestingly, some of these posterior transformation phenotypes are also present in heterozygous animals. Based on our findings, we conclude that at least some of the posterior phenotypes could be associated with misregulation of neighboring genes possibly by the drug-resistance cassette used for gene targeting (Fiering *et al.*, 1995) or by mutation of one or several of the complex regulatory elements spread along the *Hox* clusters (Gould *et al.*, 1997; Guthrie *et al.*, 1990; Sham *et al.*, 1992; Sharpe *et al.*, 1998; Whiting *et al.*, 1991).

Colinearity

The molecular mechanisms that regulate the temporal and spatial colinearity of *Hox* gene expression remain largely unknown. The *HoxB∆1* allele did not eliminate the *Hoxb13* gene, which seems to maintain colinearity properties despite the 70 kb separation from the rest of the cluster. We addressed the effects of the *HoxB∆1* deficiency on the pattern of expression of the *Hoxb13* gene. If colinearity depended on a simple sequential "chromatin opening" at a determined rate regulated by an element located 3' of the *HoxB* cluster, *Hoxb13* would be expressed at a time and with a pattern of expression similar to that of *Hoxb8* in the *HoxB∆1* mutants. Interestingly, the deletion of the *Hoxb1–Hoxb9* genes, and the consequent transposition of *Hoxb13* 90 kb closer to the genomic region on the 3' side of the *HoxB* cluster, did not seem to affect the spatial distribution of this gene's expression. This suggests that neither the physical distance between the 3' side of the cluster and *Hoxb13* nor the presence of genes and their regulatory sequences inside the deficiency is necessary for the colinear properties of *Hoxb13*. These results would be inconsistent with a model involving a sequential activation controlled by a regulatory element located on the 3' side of the cluster. The long physical distance and the presence of repetitive DNA elements between *Hoxb9* and *Hoxb13* have led to the suggestion that the colinear expression of *Hoxb13* might be regulated independent of the cluster (Zeltser *et al.*, 1996). Interestingly, a *Hoxd13* transgene resembled endogenous expression in the main body axis but not in the limbs. Previous reports have suggested the presence of a regulatory element between *Hoxd12* and *Hoxd13* directing the correct pattern of expression of *Abd B* genes in the *HoxD* cluster
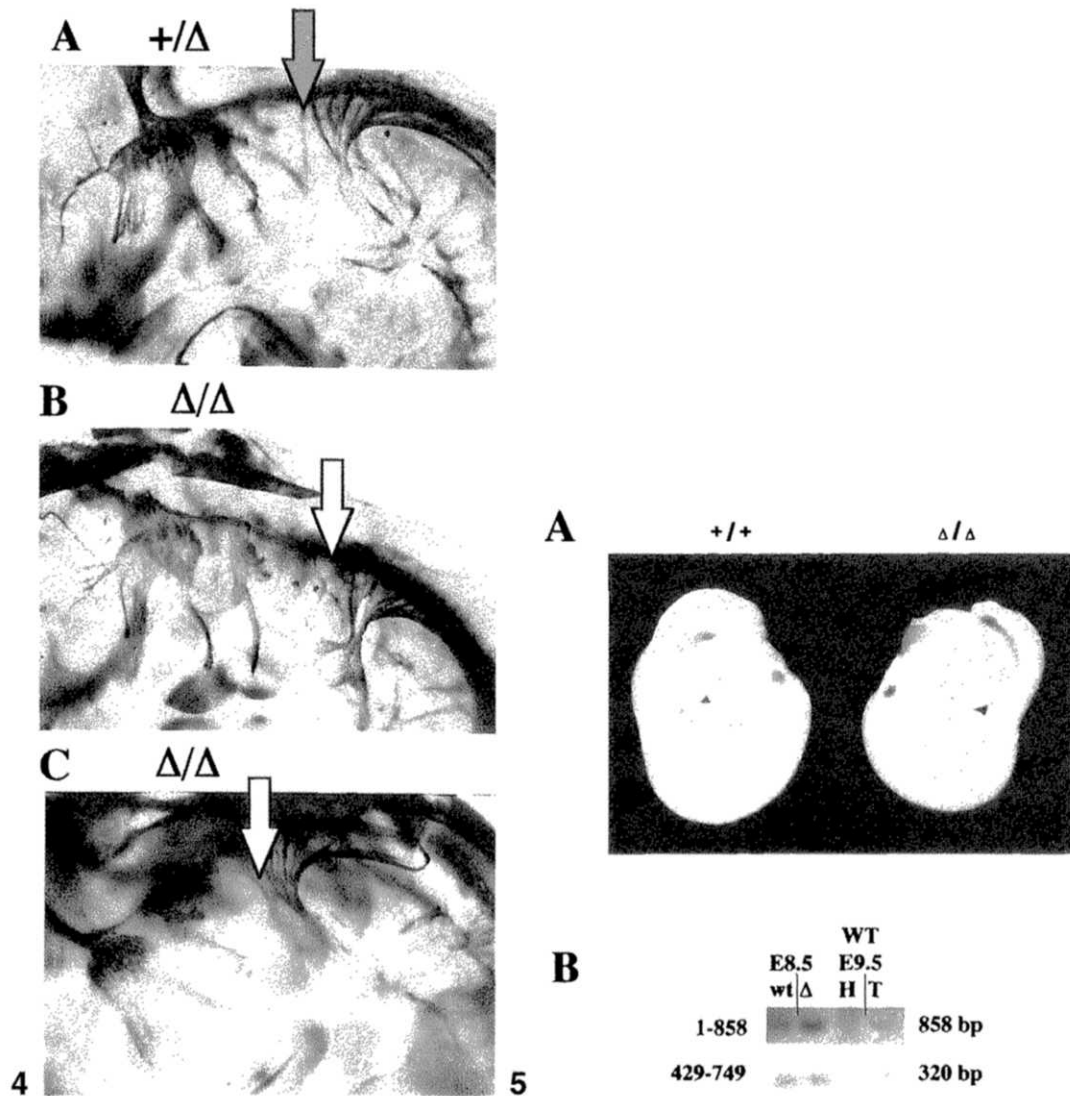
FIG. 4. Neurofilament immunostaining of cranial nerves and ganglia. (A) Heterozygous mice were indistinguishable from wild-type embryos and are used as control. The organization of trigeminal and facioacoustic ganglia is normal, and nerve IX and X fibers are clearly individualized (red arrow.) (B) *HoxBΔ1* mutant exhibiting absence of the IXth nerve and abnormal migration of Xth nerve fibers (white arrow). (C) Phenotype observed more frequently in *HoxBΔ1* mutants, note IXth nerve abnormally fused to Xth nerve.

FIG. 5. Effect of the *HoxBΔ1* allele on *Hoxb13* expression. (A) Whole-mount RNA *in situ* hybridization of *Hoxb13* expression in E9.5 *HoxBΔ1* mutant (Δ/Δ) and wild-type littermate (+/+). Expression is confined to the posterior region of the embryo in both instances. The signal in the otic vesicle is most likely an artifact since no expression was detected in the anterior part of the embryo by RT-PCR. (B) RT-PCR of *Hoxb13* at E8.5 and E9.5. Total RNA was extracted from pooled wild-type embryos (WT) or from pooled embryos of a *HoxBΔ1* heterozygous cross (Δ). E9.5 embryos were dissected into head (H) and trunk (T) parts prior to RNA purification. Two independent RT-PCRs were carried out with two different *Hoxb13*-specific sets of primers (upper and lower blots, respectively); the numbers on the left indicate the nucleotide positions of the respective primers on the *Hoxb13* cDNA. Genotypes and embryonic stages of the mRNA samples are indicated at the top. The expected sizes of the PCR products are indicated on the right. *Hoxb13* is detected at E8.5 in both wild-type and *HoxBΔ1* embryos using two different pair of primers. At E 9.5, *Hoxb13* is detected only in the trunk.

(Kondo *et al.*, 1998). Our experiment does not discard the possibility that a general regulatory element could be present in the genomic region between the end of the deletion and *Hoxb13*. Finally, we cannot exclude the pos-

sibility that *Hoxb13* expression was modified by the regulatory elements introduced in the *hprt* cassette but such an artifactual deregulation would be unlikely to produce a correct expression pattern. Thus, we conclude that the

HoxBΔ1 deletion did not involve important regulatory sequences influencing *Hoxb13* gene expression and that its expression is independent of the total distance from the 3' end of the cluster.

Relative Importance of HoxB Cluster in Pattern Formation

Hox gene expression domains in vertebrates include the paraxial mesoderm, the hindbrain, the neural tube, and the precursor tissues of the heart, kidney, gastrointestinal tract, lungs, and reproductive organs (Keynes and Krumlauf, 1994). Here, we analyzed the effect of *HoxBΔ1* in organogenesis and the patterning of the hindbrain and cranial nerves. This analysis revealed no obvious defects in organs that express *Hox* genes. Instead, phenotypes observed in the heart and thymus are probably secondary to the defects of the thoracic rib cage and the hypomorphic and split sternum. We could not document any obvious primary defects after the removal of nine genes in the *HoxB* cluster. Our findings did not reveal new or additional phenotypes in the hindbrain compared to those previously reported for the null mutation of the *Hoxb3* gene (Manley and Capecchi, 1997). This is a low penetrance phenotype involving the IXth cranial nerve, which has been also found in the *Hoxa1* homozygous mutant (Mark *et al.*, 1993), in *Hoxa1(3'RARE)* single mutants (Dupe *et al.*, 1997), and in *Hoxa1(3'RARE)/Hoxb1(3'RARE)* compound mutants (Gavalas *et al.*, 1998). We were unable to document abnormalities previously reported in the VIIth cranial nerve of *Hoxb1* and *Hoxb2* individual mutants (Studer *et al.*, 1996; Goddard *et al.*, 1996; Barrow and Capecchi, 1996). This could be due to the relatively low sensitivity of the assay used (whole-mount immunostaining) compared to histological analysis or retrograde motoneuron labeling. Clearly, a more detailed analysis of the effect of the *HoxBΔ1* deficiency is necessary to unravel its effect on hindbrain segmentation.

The most striking characteristic of the *HoxBΔ1* mutants is that despite the large extent of the deletion and its broad phenotypic range along the anteroposterior axis, no homeotic transformation extends more than one segment. Interestingly, although the mutants exhibit higher penetrance compared to most mutations in individual *HoxB* genes (Fig. 3D) (Barrow and Capecchi, 1996; Ramirez-Solis *et al.*, 1993; Rancourt *et al.*, 1995; Chen *et al.*, 1998; Chen and Capecchi, 1997) very few phenotypes shown by the *HoxBΔ1* mutants have not already been described in any one of the individual mutations. The relatively subtle effect may be due to redundant gene function mediated by the other *Hox* clusters.

Combining mutations in paralogous group 4 leads to a dosage-sensitive increase in the number of cervical vertebrae transformed toward C1 (Horan *et al.*, 1995b), and a deficiency in the unique HOM-C cluster of *Tribolium* causes the development of antennae in all body segments (Stuart *et al.*, 1991), suggesting that *Hox* genes modify a ground state to determine segmental identity. This raises the possibility that the combined loss of more clusters would result in a progressive anteriorization of segments toward a ground state, perhaps similar to C1. Since double mutation of *hoxa3* and *hoxd3* led to the deletion of C1 (Capecchi, 1996; Condie and Capecchi, 1994) the ground state could be located at the C2 level but still have C1 morphology. Chromosomal engineering of other *Hox* clusters will facilitate testing the effect of removing the *Hox* clusters from the mouse singly and in combinations to test this hypothesis.

REFERENCES

Argao, E. A., Kern, M. J., Branford, W. W., Scott, W. J., and Potter, S. S. (1995). Malformations of the heart, kidney, palate, and skeleton in alpha-mhc-hoxb-7 transgenic mice. *Mech. Dev.* **52,** 291–303.

Bailey, W. J., Kin, J., Wagner, G. P., and Ruddle, F. H. (1997). Phylogenetic reconstruction of vertebrate Hox cluster duplications. *Mol. Biol. Evol.* **14,** 843–853.

Balling, R., Mutter, G., Gruss, P., and Kessel, M. (1989). Craniofacial abnormalities induced by ectopic expression of the homeobox gene Hox-1.1 in transgenic mice. *Cell* **58,** 337–347.

Barrow, J. R., and Capecchi, M. R. (1996). Targeted disruption of the Hoxb-2 locus in mice interferes with expression of Hoxb-1 and Hoxb-4. *Development* **122,** 3817–3828.

Capecchi, M. R. (1996). Function of homeobox genes in skeletal development. *Ann. N. Y. Acad. Sci.* **785,** 34–37.

Carpenter, E. M., Goddard, J. M., Chisaka, O., Manley, N. R., and Capecchi, M. R. (1993). Loss of Hox-A1 (Hox-1.6) function results in the reorganization of the murine hindbrain. *Development* **118,** 1063–1075.

Charite, J., de Graaff, W., and Deschamps, J. (1995). Specification of multiple vertebral identities by ectopically expressed Hoxb-8. *Dev. Dyn.* **204,** 13–21.

Chen, F., and Capecchi, M. R. (1997). Targeted mutations in Hoxa-9 and Hoxb-9 reveal synergistic interactions. *Dev. Biol.* **181,** 186–196.

Chen, F., and Capecchi, M. R. (1999). Paralogous mouse Hox genes, Hoxa9, Hoxb9, and Hoxd9, function together to control development of the mammary gland in response to pregnancy. *Proc. Natl. Acad. Sci. USA* **96,** 541–546.

Chen, F., Greer, J., and Capecchi, M. R. (1998). Analysis of Hoxa7/Hoxb7 mutants suggests periodicity in the generation of the different sets of vertebrae. *Mech. Dev.* **77,** 49–57.

Chen, J. M. (1952). Studies on the morphogenesis of the mouse sternum (I. Normal embryonic development). *J. Anat.* **86,** 373–386.

Chisaka, O., and Capecchi, M. R. (1991). Regionally restricted developmental defects resulting from targeted disruption of the mouse homeobox gene hox-1.5. *Nature* **350,** 473–479. [See comments]

Chisaka, O., Musci, T. S., and Capecchi, M. R. (1992). Developmental defects of the ear, cranial nerves and hindbrain resulting from targeted disruption of the mouse homeobox gene *Hox-1.6*. *Nature* **355,** 516–520.

Condie, B. G., and Capecchi, M. R. (1993). Mice homozygous for a targeted disruption of Hoxd-3 (Hox-4.1) exhibit anterior transformations of the first and second cervical vertebrae, the atlas and the axis. *Development* **119,** 579–595.

Condie, B. G., and Capecchi, M. R. (1994). Mice with targeted disruptions in the paralogous genes *hoxa-3* and *hoxd-3* reveal synergistic interactions. *Nature* **370,** 304–307.

Davenne, M., Maconochie, M. K., Neun, R., Pattyn, A., Chambon, P., Krumlauf, R., and Rijli, F. M. (1999). Hoxa2 and Hoxb2 control dorsoventral patterns of neuronal development in the rostral hindbrain. *Neuron* **22,** 677–691.

Duboule, D., and Dolle, P. (1989). The structural and functional organization of the murine HOX gene family resembles that of Drosophila homeotic genes. *EMBO J.* **8,** 1497–1505.

Duboule, D., and Morata, G. (1994). Colinearity and functional hierarchy among genes of the homeotic complexes. *Trends Genet.* **10,** 358–364.

Dupe, V., Davenne, M., Brocard, J., Dolle, P., Mark, M., Dierich, A., Chambon, P., and Rijli, F. M. (1997). In vivo functional analysis of the Hoxa-1 3′ retinoic acid response element (3′RARE). *Development* **124,** 399–410.

Fiering, S., Epner, E., Robinson, K., Zhuang, Y., Telling, A., Hu, M., Martin, D. I., Enver, T., Ley, T. J., and Groudine, M. (1995). Targeted deletion of 5′HS2 of the murine beta-globin LCR reveals that it is not essential for proper regulation of the beta-globin locus. *Genes Dev.* **9,** 2203–2213.

Fiering, S., Kim, C. G., Epner, E. M., and Groudine, M. (1993). An "in–out" strategy using gene targeting and FLP recombinase for the functional dissection of complex DNA regulatory elements: Analysis of the β-globin locus control region. *Proc. Natl. Acad. Sci. USA* **90,** 8469–8473.

Fromental-Ramain, C., Warot, X., Lakkaraju, S., Favier, B., Haack, H., Birling, C., Dierich, A., Dollé, P., and Chambon, P. (1996). Specific and redundant functions of the paralogous Hoxa-9 and Hoxd-9 genes in forelimb and axial skeleton patterning. *Development* **122,** 461–472.

García-Fernández, J., and Holland, P. W. H. (1994). Archetypal organization of the amphioxus Hox gene cluster. *Nature* **370,** 563–566.

Gaunt, S., Sharpe, P., and Duboule, D. (1988). Spatially restricted domains of homeo-gene transcripts in mouse embryos: Relation to a segmented body plan. *Development Suppl.* **104,** 169–179.

Gaunt, S. J., Krumlauf, R., and Duboule, D. (1989). Mouse homeo-genes within a subfamily, Hox-1.4, -2.6 and -5.1, display similar anteroposterior domains of expression in the embryo, but show stage- and tissue-dependent differences in their regulation. *Development* **107,** 131–141.

Gavalas, A., Studer, M., Lumsden, A., Rijli, F. M., Krumlauf, R., and Chambon, P. (1998). Hoxa1 and Hoxb1 synergize in patterning the hindbrain, cranial nerves and second pharyngeal arch. *Development* **125,** 1123–1136.

Goddard, J. M., Rossei, M., Manley, N. R., and Capecchi, M. R. (1996). Mice with targeted disruption of Hoxb-1 fail to form the motor nucleus of the VIIth nerve. *Development* **122,** 3217–3228.

Godwin, A., and Capecchi, M. (1998). Hoxc13 mutant mice lack external hair. *Genes Dev.* **12,** 11–20.

Gould, A., Morrison, A., Sproat, G., White, R. A., and Krumlauf, R. (1997). Positive cross-regulation and enhancer sharing: Two mechanisms for specifying overlapping Hox expression patterns. *Genes Dev.* **11,** 900–913.

Graham, A., Papalopulu, N., and Krumlauf, R. (1989). The murine and Drosophila homeobox gene complexes have common features of organization and expression. *Cell* **57,** 367–378.

Guthrie, S., Muchamore, I., Kuroiwa, A., Marshall, H., Krumlauf, R., and Lumsden, A. (1990). Alternatively spliced Hox-1.7 transcripts encode different protein products. *DNA Seq.* **1,** 115–124.

Horan, G., Kovacs, E., Behringer, R., and Featherstone, M. (1995a). Mutations in paralogous Hox genes result in overlapping homeotic transformations of the axial skeleton: Evidence for unique and redundant function. *Dev. Biol.* **169,** 359–372.

Horan, G., Ramirez-Solis, R., Featherstone, M., Wolgemuth, D., Bradley, A., and Behringer, R. (1995b). Compound mutants for the paralogous *hoxa-4, hoxb-4,* and *hoxd-4* genes show more complete homeotic transformations and a dose-dependent increase in the number of vertebrae transformed. *Genes Dev.* **9,** 1667–1677.

Horan, G. S., Wu, K., Wolgemuth, D. J., and Behringer, R. R. (1994). Homeotic transformation of cervical vertebrae in Hoxa-4 mutant mice. *Proc. Natl. Acad. Sci. USA* **91,** 12644–12648.

Jeannotte, L., Lemieux, M., Charron, J., Poirier, F., and Robertson, E. J. (1993). Specification of axial identity in the mouse: Role of the Hoxa-5 (Hox1.3) gene. *Genes Dev.* **7,** 2085–2096.

Kappen, C., Schughart, K., and Ruddle, F. (1989). Two steps in the evolution of Antennapedia-class vertebrate homeobox genes. *Evolution* **86,** 5459–5463.

Kessel, M., Balling, R., and Gruss, P. (1990). Variations of cervical vertebrae after expression of a *Hox-1.1* transgene in mice. *Cell* **61,** 301–308.

Kessel, M., and Gruss, P. (1991). Homeotic transformations of murine vertebrae and concomitant alteration of Hox codes induced by retinoic acid. *Cell* **67,** 89–104.

Keynes, R., and Krumlauf, R. (1994). Hox genes and regionalization of the nervous system. *Annu. Rev. Neurosci.* **17,** 109–132.

Kondo, T., and Duboule, D. (1999). Breaking colinearity in the mouse HoxD complex. *Cell* **97,** 407–417.

Kondo, T., Zákány, J., and Duboule, D. (1998). Control of colinearity in AbdB genes of the mouse HoxD complex. *Mol. Cell* **1,** 289–300.

Kostic, D., and Capecchi, M. R. (1994). Targeted disruptions of the murine Hoxa-4 and Hoxa-6 genes result in homeotic transformations of components of the vertebral column. *Mech. Dev.* **46,** 231–247.

Krumlauf, R. (1994). Hox genes in vertebrate development. *Cell* **78,** 191–201.

Le Mouellic, H., Lallemand, Y., and Brulet, P. (1992). Homeosis in the mouse induced by a null mutation in the *Hox-3.1* gene. *Cell* **69,** 251–264.

Lewis, E. (1978). A gene complex controlling segmentation in Drosophila. *Nature* **276,** 565–570.

Liu, P., Zhang, H., McLellan, A., Vogel, H., and Bradley, A. (1998). Embryonic lethality and tumorigenesis caused by segmental aneuploidy on mouse chromosome 11. *Genetics* **150,** 1155–1168.

Lufkin, T., Dierich, A., LeMeur, M., Mark, M., and Chambon, P. (1991a). Disruption of the Hox-1.6 homeobox gene results in defects in a region corresponding to its rostral domain of expression. *Cell* **66,** 1105–1119.

Lufkin, T., Dierich, A., LeMeur, M., Mark, M., and Chambon, P. (1991b). Homeotic transformations of murine vertebrae and concomitant alteration of Hox codes induced by retinoic acid. *Cell* **67**, 89–104.

Lufkin, T., Mark, M., Hart, C., Dolle, P., Lemeur, M., and Chambon, P. (1992). Homeotic transformation of the occipital bones of the skull by ectopic expression of a homeobox gene. *Nature* **359**, 835–841.

Manley, N., and Capecchi, M. (1997). Hox group 3 paralogous genes act synergistically in the formation of somitic and neural crest-derived structures. *Dev. Biol.* **192**, 274–288.

Manley, N. R., and Capecchi, M. R. (1995). The role of Hoxa-3 in mouse thymus and thyroid development. *Development* **121**, 1989–2003.

Manley, N. R., and Capecchi, M. R. (1998). Hox group 3 paralogs regulate the development and migration of the thymus, thyroid, and parathyroid glands. *Dev. Biol.* **195**, 1–15.

Mark, M., Lufkin, T., Vonesch, J., Ruberte, E., Olivo, J., Dolle, P., Gorry, P., Lumsden, A., and Chambon, P. (1993). Two rhombomeres are altered in Hoxa-1 mutant mice. *Development* **119**, 319–338.

McLain, K., Schreiner, C., Yager, K. L., Stock, J. L., and Potter, S. S. (1992). Ectopic expression of *Hox-2.3* induces craniofacial and skeletal malformations in transgenic mice. *Mech. Dev.* **39**, 3–16.

Mortlock, D. P., Post, L. C., and Innis, J. W. (1996). The molecular basis of hypodactyly (*Hd*): A deletion in Hoxa13 leads to arrest of digital arch formation. *Nat. Genet.* **13**, 284–289.

Muragaki, Y., Mundlos, S., Upton, J., and Olsen, B. J. (1996). Altered growth and branching patterns in synpolydactyly caused by mutations in HOXD13. *Science* **272**, 548–551.

Nurten Akarsu, A., Stoilov, I., Yilmaz, E., Sayli, B. S., and Sarfarazi, M. (1996). Genomic structure of *HOXD13* gene: A nine polyalanine duplication causes synpolydactyly in two unrelated families. *Hum. Mol. Genet.* **5**, 945–952.

Ramirez Solis, R., Zheng, H., Whiting, J., Krumlauf, R., and Bradley, A. (1993). *Hoxb-4 (Hox-2.6)* mutant mice show homeotic transformation of a cervical vertebra and defects in the closure of the sternal rudiments. *Cell* **73**, 279–294.

Ramirez-Solis, R., Davis, A. C., and Bradley, A. (1993). Gene targeting in embryonic stem cells. *Methods Enzymol.* **225**, 855–878.

Ramirez-Solis, R., Liu, P., and Bradley, A. (1995). Chromosome engineering in mice. *Nature* **378**, 720–724.

Ramirez-Solis, R., Rivera, J., Wallace, J., Wims, M., Zheng, H., and Bradley, A. (1992). Genomic DNA microextraction: A method to screen numerous samples. *Anal. Biochem.* **201**, 331–335.

Rancourt, D. E., Tsuzuki, T., and Capecchi, M. R. (1995). Genetic interaction between *hoxb-5* and *hoxb-6* is revealed by nonallelic noncomplementation. *Genes Dev.* **9**, 108–122.

Rijli, F. M., Dolle, P., Fraulob, V., LeMeur, M., and Chambon, P. (1994). Insertion of a targeting construct in a Hoxd-10 allele can influence the control of Hoxd-9 expression. *Dev. Dyn.* **201**, 366–377.

Rijli, F. M., Mark, M., Lakkaraju, S., Dierich, A., Dolle, P., and Chambon, P. (1993). A homeotic transformation is generated in the rostral branchial region of the head by disruption of Hoxa-2, which acts as a selector gene. *Cell* **75**, 1333–1349.

Rubock, M. J., Larin, Z., Cook, M., Papalopulu, N., Krumlauf, R., and Lehrach, H. (1990). A yeast artificial chromosome containing the mouse homeobox cluster *Hox-2. Proc. Natl. Acad. Sci. USA*

87, 4751–4755. [Published erratum appears in *Proc. Natl. Acad. Sci. USA*, 1990, **87**, 7346]

Saegusa, H., Takahashi, N., Noguchi, S., and Suemori, H. (1996). Targeted disruption in the mouse Hoxc-4 locus results in axial skeleton homeosis and malformation of the xiphoid process. *Dev. Biol.* **174**, 55–64.

Sham, M. H., Hunt, P., Nonchev, S., Papalopulu, N., Graham, A., Boncinelli, E., and Krumlauf, R. (1992). Analysis of the murine *Hox-2.7* gene: Conserved alternative transcripts with differential distributions in the nervous system and the potential for shared regulatory regions. *EMBO J.* **11**, 1825–1836.

Sharpe, J., Nonchev, S., Gould, A., Whiting, J., and Krumlauf, R. (1998). Selectivity, sharing and competitive interactions in the regulation of Hoxb genes. *EMBO J.* **17**, 1788–1798.

Small, K. M., and Potter, S. S. (1993). Homeotic transformations and limb defects in Hox A11 mutant mice. *Genes Dev.* **7**, 2318–2328.

Stuart, J. J., Brown, S. J., Beeman, R. W., and Denell, R. E. (1991). A deficiency of the homeotic complex in the beetle *Tribolium. Nature* **350**, 72–74.

Studer, M., Lumsden, A., Ariza-McNaughton, L., Bradley, A., and Krumlauf, R. (1996). Altered segmental identity and abnormal migration of motor neurons in mice lacking *Hoxb-1. Nature* **384**, 630–634.

Suemori, H., Takahashi, N., and Noguchi, S. (1995). Hoxc-9 mutant mice show anterior transformation of the vertebrae and malformation of the sternum and ribs. *Mech. Dev.* **51**, 265–273.

van der Hoeven, F., Zakany, J., and Duboule, D. (1996). Gene transpositions in the HoxD complex reveal a hierarchy of regulatory controls. *Cell* **85**, 1025–1035.

Wall, N. A., Jones, C. M., Hogan, B. L. M., and Wright, C. V. E. (1992). Expression and modification of Hox-2.1 protein in mouse embryos. *Mech. Dev.* **37**, 111–120.

Whiting, J., Marshall, H., Cook, M., Krumlauf, R., Rigby, P. W. J., Stott, D., and Allemann, R. K. (1991). Multiple spatially specific enhancers are required to reconstruct the pattern of *Hox-2.6* gene expression. *Genes Dev.* **5**, 2048–2059.

Wilkinson, D. G., and Nieto, M. A. (1993). Detection of messenger RNA by in situ hybridization to tissue sections and whole mounts. *Methods Enzymol.* **225**, 361–373.

Wolgemuth, D. J., Behringer, R. R., Mostoller, M. P., Brinster, R. L., and Palmiter, R. D. (1989). Transgenic mice overexpressing the mouse homeobox-containing gene Hox-1.4 exhibit abnormal gut development. *Nature* **337**, 464–467.

Wright, C. V. E., Cho, K. W. Y., Hardwicke, J., Collins, R. H., and De Robertis, E. M. (1989). Interference with function of a homeobox gene in *Xenopus* embryos produces malformations of the anterior spinal cord. *Cell* **59**, 81–93.

Zakany, J., and Duboule, D. (1996). Synpolydactyly in mice with a targeted deficiency in the HoxD complex. *Nature* **384**, 69–71.

Zakany, J., Gerard, M., Favier, B., and Duboule, D. (1997). Deletion of a HoxD enhancer induces transcriptional heterochrony leading to transposition of the sacrum. *EMBO J.* **16**, 4393–4402.

Zeltser, L., Desplan, C., and Heintz, N. (1996). *Hoxb-13:* A new Hox gene in a distant region of the HOXB cluster maintains colinearity. *Development* **122**, 2475–2484.